Available online at www.sciencedirect.com
ScienceDirect
Journal of Photochemistry and Photobiology A: Chemistry 190 (2007) 101–109
Journal of Photochemistry and Photobiology A:Chemistry
www.elsevier.com/locate/jphotochem

Intermolecular exciplex formation and photoinduced electron transfer of 1,8-naphthalimide dyads in methylated benzenes

Dae Won Cho [a,b], Mamoru Fujitsuka [a], Ung Chan Yoon [c], Tetsuro Majima [a,*]

[a] *The Institute of Scientific and Industrial Research, Osaka University, Mihogaoka 8-1, Ibaraki, Osaka 567-0047, Japan*
[b] *Department of Chemistry, Chosun University, Gwangju 501-759, Republic of Korea*
[c] *Department of Chemistry, Pusan National University, Pusan 609-735, Republic of Korea*

Received 9 January 2007; received in revised form 19 March 2007; accepted 19 March 2007
Available online 23 March 2007

Abstract

In methylated benzene (MB) solvents, 1,8-naphthalimide (NI) derivatives showed markedly red-shifted emission, which originated from an intermolecular exciplex formation between NI and MB in the singlet excited state. The exciplex emission shifted to longer wavelength according to an increase of the oxidation potential of MB. The Stokes shift of the exciplex emission obeyed Lippert–Mataga theory. On the other hand, the exciplex emission of 1,8-naphthalimide-linker-phenothiazine (NI-L-PTZ) dyads was markedly quenched by the linked PTZ. The transient absorption measurements were carried out to investigate the fast quenching process on NI-L-PTZ dyads in *p*-XYL/CH_3CN. The NI radical ion is predominantly generated from the photoinduced electron transfer (PET) between the singlet excited NI and PTZ. The quantum yields for PET of NI-L-PTZ dyads in *p*-XYL/CH_3CN were smaller than those in pure CH_3CN. This indicates that the exciplex formation of NI-L-PTZ dyads with MB competitively occurs with the PET process.

Keywords: 1,8-Naphthalimide; Exciplex; Photoinduced electron transfer; Methylated benzene; Phenothiazine

1. Introduction

1,8-Naphthalimide (NI) derivatives have been received considerable attention for both their photophysical properties and potential applications in biology [1–3]. Since NI derivatives have excellent electron-acceptor property, they have been used in many studies of the photoinduced electron transfer (PET) involving various electron donors [1–4]. Moreover, the covalently linked NI dyads with electron donor are often used to mimic the PET processes in natural systems [5,6]. On the other hands, the photophysical properties of NI derivatives have been mostly studied in polar solvents such as acetonitrile or water, because of their PET applications [7–10].

In the previous work, we have prepared well-designed NI dyads, in which effects of the linkers between the electron-donating phenothiazine (PTZ) moiety and the NI moiety were examined [4]. Especially, we have studied the photophysical properties of NI derivatives in nonpolar solvents [11]. In *n*-hexane, we observed that the intermolecular excimer formation between two NI molecules and the intramolecular exciplex formation in NI dyads with PTZ [11]. However, the formation of these dimers (excimer and/or exciplex) in the excited state was inhibited by toluene as the solvent. Furthermore, the emission spectral properties of NI in toluene are different from that in *n*-hexane, which cannot be explained by the general solvent-polarity effect. We suggested that NI forms the exciplex with toluene molecule, showing the peculiar photophysical properties [4].

In order to clear up this point on the NI properties in toluene, we focus our attention on other aromatic donors (methylated benzene moelcules, MB) with a series of oxidation potentials as shown in Scheme 1 (aromatic donors in Scheme 1 are in the order of donor strength). We found the exciplex formation of NI with MB molecules. However, the formation of exciplex in NI-L-PTZ dyads was found to be inhibited by the PET process. The PET process in NI-L-PTZ is competitive with the exciplex formation process. For this study, we synthesized various NI derivatives (NI-C1, NI-C7, NI-O, NI-O3, NI-S and NI-SOS)

* Corresponding author.
E-mail address: majima@sanken.osaka-u.ac.jp (T. Majima).

1010-6030/$ – see front matter © 2007 Elsevier B.V. All rights reserved.
doi:10.1016/j.jphotochem.2007.03.018

Acceptor

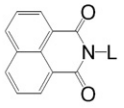

NI-L

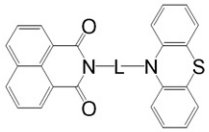

NI-L-PTZ

compounds	linkers (L)
NI-C	$-CH_3$
NI-C7	$-(CH_2)_6-CH_3$
NI-O	$-(CH_2)_2-O-CH_2CH_3$
NI-O3	$-(CH_2)_2-O-(CH_2)_2-O-(CH_2)_2-O-CH_2CH_3$
NI-S	$-(CH_2)_2-S-CH_2CH_3$
NI-SOS	$-(CH_2)_2-S-(CH_2)_2-O-(CH_2)_2-S-CH_2CH_3$
NI-C8-PTZ	$-(CH_2)_8-$
NI-C11-PTZ	$-(CH_2)_{11}-$
NI-O-PTZ	$-(CH_2)_2-O-(CH_2)_2-O-(CH_2)_2-O-(CH_2)_2-$

Donor

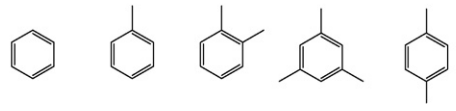

	BZ	TOL	o-XYL	TMB	p-XYL
E°_{ox}(V vs.SCE) [a]	2.7	2.42	2.13	2.11	2.01
ε [b]	2.284	2.379	2.568	2.279	2.270

Scheme 1. (a) Oxidation potential (*V vs.* SCE) values from ref. [12]. (b) Dielectric constants (ε) from ref. [13].

in order to reveal the effect of different substitutes as shown in Scheme 1. Furthermore, we prepared NI dyads, which have three kinds of linkers (L) between the electron-donating PTZ moiety and the electron-accepting NI moiety, *i.e.* NI-L-PTZ such as NI-C8-PTZ, NI-C11-PTZ, and NI-O-PTZ, where L is octanyl (C8), undecyl (C11) and trioxaundecanyl (O), respectively [4,11].

2. Experimental

2.1. Materials

The details of synthesis of the dyads (*N*-(8-phenothiazinyloctyl)-1,8-naphthalimide (NI-C8-PTZ), *N*-(11-phenothiazinylundecyl)-1,8-naphthalimide (NI-C11-PTZ), *N*-(11-phenothiazinyl-3,6,9-trioxaundecyl)-1,8-naphthalimide (NI-O-PTZ)), and reference NI molecules (*N*-methyl-1,8-naphthalimide (NI-C), *N*-heptyl-1,8-naphthalimide (NI-C7), *N*-(2-methoxylethyl)-1,8-naphthalimide (NI-O), *N*-(3,6,9-trioxaundecyl)-1,8-naphthalimide (NI-O3), *N*-(2-methylthioethyl)-1,8-naphthalimide (NI-S), and *N*-(3,9-dithio-6-oxa-undecyl)-1,8-naphthalimide (NI-SOS)) have been described earlier [4,11]. All solvents (acetonitrile (CH_3CN), benzene (BZ), toluene (TOL), *o*-xylene (*o*-XYL), 1,3,5-trimethylbenzene (TMB), *p*-xylene (*p*-XYL)) were the fluorescence spectroscopic grade and used without further purification.

2.2. Spectroscopic measurements

Steady-state UV–vis absorption spectra were recorded with a UV–vis spectrophotometer (Shimadzu UV-3100) at room temperature. Fluorescence spectra were measured using a Hitachi 850 fluorophotometer. Fluorescence quantum yields (ϕ_f) were estimated using a toluene solution of anthracene as a standard with a known value of $\phi_f = 0.30$ [13].

Time-resolved fluorescence spectra were measured by the single photon counting method [14], using a streakscope (Hamamatsu Photonics, C4334-01) equipped with a polychromator (Acton Research, SpectraPro150). Ultrashort laser pulse was generated with a titanium:sapphire laser (Spectra-Physics, Tsunami 3941-M1BB, fwhm 100 fs) pumped with a diode-pumped solid-state laser (Spectra-Physics, Millennia VIIIs). For excitation of the sample, the output of the Ti:sapphire laser was converted to third harmonic generation (THG, 300 nm) with a harmonic generator (Spectra-Physics, GWU-23FL).

The sub-picosecond transient absorption spectra were measured by the pump and probe method using a regeneratively amplified titanium sapphire laser (Spectra-Physics, Spitfire Pro F, 1 kHz) pumped by a Nd:YLF laser (Spectra-Physics, Empower 15). The seed pulse was generated by a titanium sapphire laser. The fourth harmonic generation (330 nm, 5 $\mu J\,pulse^{-1}$) of the optical parametric amplifier (Spectra-Physics, OPA-800CF-1) was used as the excitation pulse. A white light continuum pulse, which was generated by focusing the residual of the fundamental light to the flowing water cell after the computer-controlled optical delay, was divided into two parts and used as the probe and the reference lights, of which latter was used to compensate the laser fluctuation. The both probe and reference lights were directed to the rotating sample cell with 1.0 mm of optical path and detected with the CCD detector equipped with the polychromator (Solar, MS3504). The pump pulse was chopped by the mechanical chopper synchronized to one-half of the laser repetition rate, resulting in a pair of the spectra with and without the pump, from which absorption change induced by the pump pulse was estimated.

Nanosecond transient absorption measurements were carried out by employing the technique of laser flash photolysis. The THG (355 nm) of Q-switched Nd:YAG laser (Brilliant, pulse width of 5-ns fwhm) was used to excite the NI moiety selectively, because it has strong absorption around 355 nm, while PTZ has no absorption at wavelength longer than 320 nm. Pulse energy was *ca.* 18 $mJ\,pulse^{-1}$. A Xenon flash lamp (Osram, XBO-450) was focused into the sample solution as the probe light for the transient absorption measurement. Transient absorption and temporal profiles were measured with a monochromator (Nikon, G250) equipped with a photomultiplier (Hamamatsu Photonics, R928) and a digital oscilloscope (Tektronix, TDS-580D). Reported signals were averages of 4 events. All solutions were argon-saturated unless otherwise indicated.

The quantum yields of the triplet-state formation (ϕ_T) were determined by an actinometry using benzophenone (6500 $M^{-1}cm^{-1}$ at 520 nm, $\phi_T = 1$) in CH_3CN as a standard [15]. The extinction coefficients of NI-C1 in the triplet-excited

state (NI(T_1)) was determined to be 5100 M^{-1} cm^{-1} at 470 nm [16,17].

3. Results and discussion

3.1. Absorption and fluorescence spectral properties

Fig. 1 shows the absorption spectra of NI-SOS and NI-C7 in various solvents. The absorption spectra of the reference NI derivatives (NI-C, NI-C7, NI-O, NI-O3, NI-S and NI-SOS) in various MB solvents showed a maximum around 332–334 nm and a shoulder around 320 nm. The absorption spectra of NI-L-PTZ dyads were almost identical to those of the reference NI derivatives and previously reported NI derivatives [18]. This result implies that there is no substantial interaction between NI and PTZ of NI-L-PTZ in the ground state. In contrast to the weak solvent-dependence in absorption spectra, the emissions of NI-SOS and NI-C7 are markedly red-shifted in order of BZ < TOL < *o*-XYL < TMB < *p*-XYL as shown in Fig. 1. The emission spectral features for other NI derivatives showed the similar spectral trends as summarized in Table 1.

In pure CH_3CN, it is noteworthy that the fluorescence spectra of NI-SOS and NI-C7 with a maximum at around 380 nm have the vibrational structure exhibiting a mirror-image to the absorption spectra as shown in Fig. 1 [11]. In MB solvents, however, there is the lack of mirror image between absorption and emission spectra of NI derivatives. In addition, the emission spectra of all NI derivatives were broaden and shifted to longer wavelength in MB solvents.

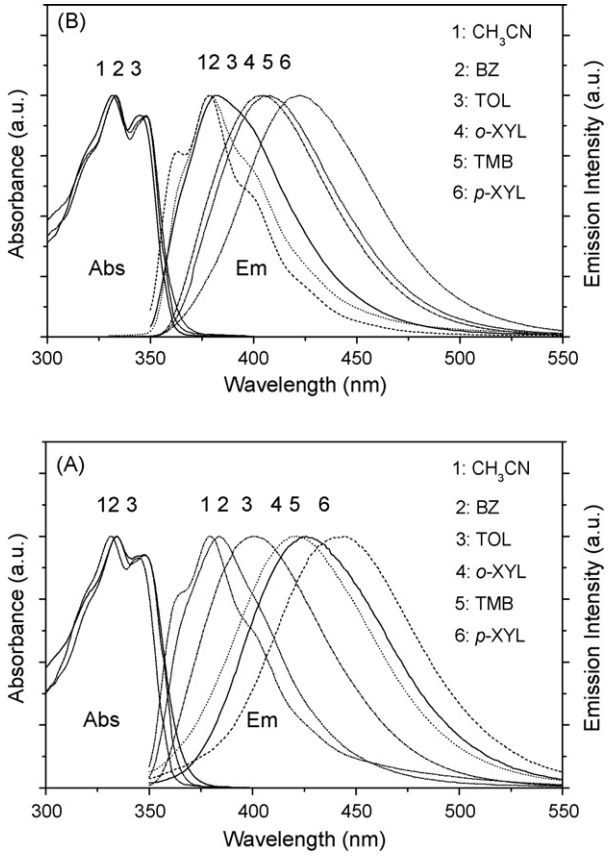

Fig. 1. Normalized absorption and emission spectra of (A) NI-SOS, and (B) NI-C7 in various solvents. CH_3CN, acetonitrile; BZ, benzene; TOL, toluene; *o*-XYL, *o*-xylene; TMB, 1,3,5-trimethylbenzene; *p*-XYL, *p*-xylene. Excitation wavelength was 320 nm.

Table 1
Fluorescence maxima (λ_{em} (nm)) and dipole moment changes ($\Delta\mu$) of NI derivatives in various methylated benzene solvents

NI derivatives	λ_{em} (nm)					$\Delta\mu$[a] (Debye)
	BZ	TOL	*o*-XYL	TMB	*p*-XYL	
NI-C8-PTZ	378	382	404	409	423	3.0
NI-C11-PTZ	379	383	405	416	427	3.1
NI-O-PTZ	379	386	408	414	428	3.6
NI-C	379	384	404	409	423	3.3
NI-C7	378	383	404	408	422	3.3
NI-O	380	384	411	412	430	4.0
NI-O3	380	387	411	415	430	4.3
NI-S	379	388	408	410	425	4.0
NI-SOS	379	400	420	425	443	4.5

Abbreviated letters indicated as follows: BZ, benzene; TOL, toluene; *o*-XYL, *o*-xylene; TMB, 1,3,5-trimethylbenzene; *p*-XYL, *p*-xylene.
[a] $\Delta\mu$ values were determined for (NI:*p*-XYL) exciplex.

We have reported the fluorescence emission of NI derivatives around 367 nm in *n*-hexane [11]. Considering the solvent polarity ($\varepsilon = 1.89$ (*n*-hexane) and $\varepsilon = 37.5$ (CH_3CN)), the red-shift of fluorescence in CH_3CN can be regarded as a common solvent effect. Furthermore, the structured emission in both *n*-hexane and CH_3CN is the mirror-image of the absorption spectra of NIs. However, the Stokes shift in MB solvents showed no correlation with the solvent polarity parameter. Although the dielectric constants ($\varepsilon = 2.27$–2.57) of used MB solvents are similar to that of *n*-hexane (Scheme 1), the emission maximum of NI in MB solvents are observed at longer wavelength compared with that in *n*-hexane or CH_3CN. This distinct Stokes-shift in MB solvents can be explained in terms of the exciplex formation. This assumption is consistent with the general tendency about the exciplex formation, for example, the diminishing of vibrational structure in the emission spectrum due to the fact that the exciplex between solute NI and aromatic MB solvent having no ground state stabilization.

There is no correlation between the emission shift and the dielectric constant of used MB solvents, but the emission maxima of the exciplex showed a linear correlation with the oxidation potential (E^o_{ox}) of MB solvents (listed in Scheme 1, and Fig. 2). Among studied MB solvents, *p*-XYL has the lowest E^o_{ox} value. Therefore, the exciplex emission in *p*-XYL showed the largest Stokes shifts (6500–7500 cm^{-1}) comparing in other MB solvents. The formation of exciplex can be attributed to the shift of a charge density from donor (MB) to acceptor (NI) concerned with the reorganization of reactant and medium. Moreover, the stabilization of exciplex is largely affected by the donor/acceptor electronic interaction energy in the excited state. Namely, the resonance (exchange) integral, which represents the donor–acceptor electronic interaction energy in exciplex sphere, depends on the aromatic MB donor strength. However, it is noticeable that the E^o_{ox} value of benzene is too high to form

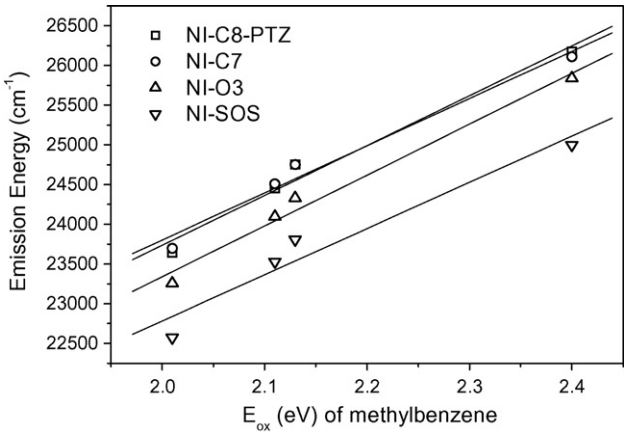

Fig. 2. Plots of the emission maxima of NI derivatives *vs.* oxidation potentials of various methylated benzenes.

the charge transfer exciplex. Thus, we did not show the data point about benzene in Fig. 2.

3.2. Singlet-state quenching by p-XYL

The emission band at 390 nm of NI-C7, which has been attributed to the excited monomer state, is markedly quenched upon addition of *p*-XYL in the concentration range of 0–0.74 M, as shown in Fig. 3. Concomitantly, a new emission band at around 450 nm is observed with increasing concentration of *p*-XYL, exhibiting an isoemissive point at 390 nm. This broad emission at longer wavelength can be assigned to the exciplex between NI-C7 and *p*-XYL. A similar quenching experiment has been carried out on other NI derivatives in CH_3CN. In these cases we observed a similar tendency, indicating the exciplex formation of NI derivatives with *p*-XYL.

The fluorescence quenching data shown in Fig. 3 were fitted to a Stern–Volmer quenching model (Eq. (1)).

$$\frac{I_0}{I} = 1 + K_q[Q] = 1 + k_s\tau_s[Q] \quad (1)$$

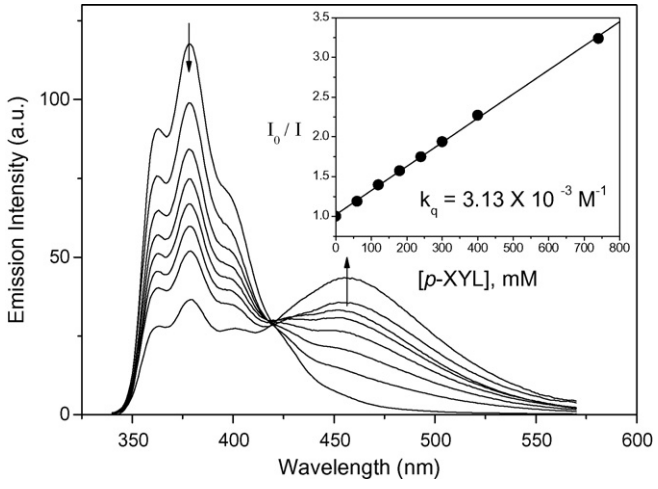

Fig. 3. The emission spectra of NI-C7 (4×10^{-5} M in CH_3CN) in presence of 0, 60, 120, 180, 240, 300, 400, and 740 mM *p*-XYL (λ_{ex} = 330 nm). Insert shows Stern–Volmer plot for quenching of ^{1}NI-C7* by *p*-XYL.

Table 2
Summary of Stern–Volmer constants and bimolecular quenching constants of NI derivatives and *p*-XYL

NI derivatives	K_q ($\times 10^3$ M^{-1})	k_s ($\times 10^{-7}$ M^{-1} s^{-1})
NI-C8-PTZ	2.03	2.39
NI-C11-PTZ	3.20	2.67
NI-O-PTZ	3.07	2.69
NI-C	4.46	2.29
NI-C7	3.13	2.27
NI-O	3.84	2.00
NI-O3	9.91	2.10
NI-S	3.89	2.40
NI-SOS	4.15	2.08

In Eq. (1), I_0 and I are the fluorescence intensities in the absence and presence of *p*-XYL quencher (Q), respectively. K_q is the Stern–Volmer quenching constant, k_s the bimolecular rate constant for quenching of ^{1}NI* by *p*-XYL, and τ_s is the lifetime of ^{1}NI*. Stern–Volmer plot for quenching by *p*-XYL is shown in the insert of Fig. 3. In all cases of NI derivatives, linear Stern–Volmer plots are obtained. Singlet lifetimes are listed in Table 3. From the slopes (Stern–Volmer constant) of the plots, along with the singlet-state lifetime, bimolecular rate constants for the quenching of ^{1}NI* by the *p*-XYL were obtained. The bimolecular rate constants are summarized in Table 2. The bimolecular rate constants of 2.00×10^7 to 2.69×10^7 M^{-1} s^{-1} were estimated for this exciplex formation. It is noticeable that the estimated bimolecular rate-constants are similar to each other. It was suggested that the linkers or side chains attached with NI are not a significant factor for the formation of exciplex. Thus, the diffusional quenching (or the formation of exciplex) by *p*-XYL is observed at slightly high concentration of *p*-XYL.

3.3. Effect of solvent polarity for exciplexes formed with p-XYL

Fig. 4(A) shows the emission spectra of NI-O3 measured in a mixture of 1,4-dioxane and CH_3CN including 5% of *p*-XYL. All NI derivatives showed two characteristic emission bands under the condition of Fig. 4; the fluorescence at around 380 nm is due to the emission from NI in the singlet excited state (^{1}NI*), and the longer emission is originated from (*p*-XYL:NI)* exciplex. The exciplex emission showed the dependence on the polarity of solvent. In the case of (*p*-XYL:NI)*-O3 exciplex, the emission maximum of the exciplex shifted to longer wavelength from 437 nm in 1,4-dioxane to 462 nm in CH_3CN (Fig. 4(A)). The monomer emission showed a little red-shift of 5 nm, which is in accordance with the fact that the NI compounds hardly showed any fluorescence peak shift with the change of solvent polarity as illustrated in the previous work [18].

However, the exciplex emissions showed outstanding solvatochromic properties. It is known that the solvent-polarity effect can be analyzed in terms of difference in the dipole moments in the ground and excited states, and it has been found that the larger dipole-moment change causes larger peak shift. This phenomenon can be analyzed by a Lippert–Mataga plot, which is essentially a plot of the Stokes shift of the fluorescence emis-

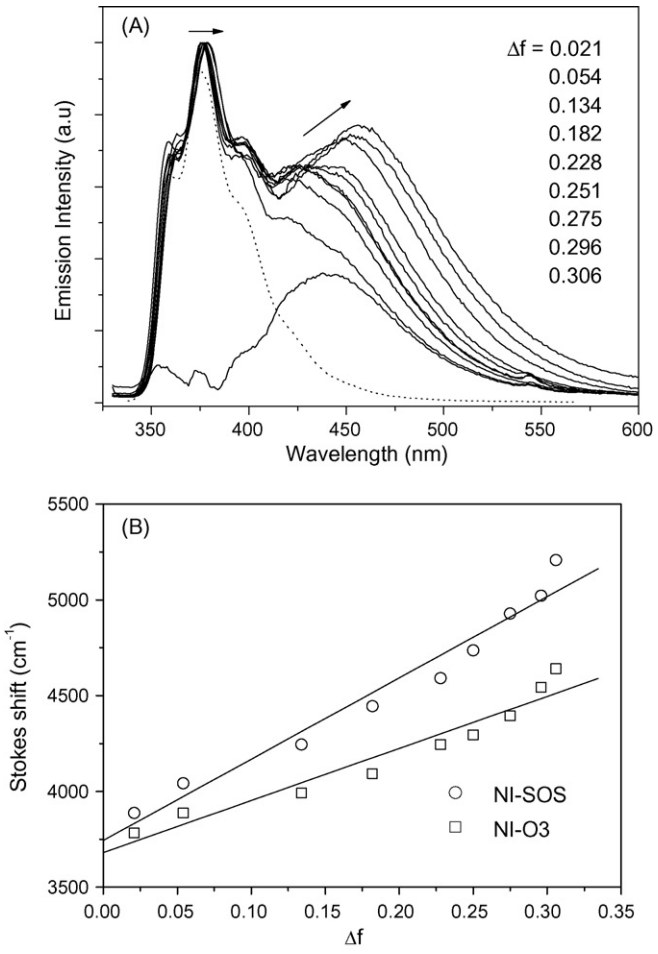

Fig. 4. (A) Emission spectra of NI-O3 in a series of 1,4-dioxane/CH_3CN mixtures. All samples were containing 5% *p*-XYL. Δf was obtained for each mixture using ε and n values calculated using the molar fractions as following: $\varepsilon = \chi_{acetonitrile} \times 38.8 + \chi_{dioxane} \times 2.218$; $n = \chi_{acetonitrile} \times 1.3442 + \chi_{dioxane} \times 1.4224$. The Δf can be easily controlled by mole fraction of dioxane; Δf ($\chi_{dioxane}$) = 0.021 (1), 0.054 (0.99), 0.134 (0.95), 0.182 (0.9), 0.228 (0.8), 0.251 (0.7), 0.275 (0.5), 0.296 (0.2) and 0.306 (0). Dotted lines show the spectra after decomposition of the spectrum for the first mixture (Δf ($\chi_{dioxane}$) = 0.021). (B) Lippert–Mataga plot of NI-O3 (squares) and NI-SOS (circles) in a series of 1,4-dioxane/CH_3CN mixtures. The lines correspond to the best linear fits to the data.

sion *versus* the solvent polarity. The difference in the absorption and emission maxima in wavenumbers ($\Delta\nu$) is expressed as the following Eq. (2):

$$\nu_a - \nu_f = \left(\frac{2}{hca_0^3}\right) \times \left(\frac{\varepsilon - 1}{2\varepsilon + 1} - \frac{n - 1}{2n + 1}\right) \times (\mu_e - \mu_g)^2 = \frac{2\Delta f}{hca_0^3}\Delta\mu^2 \quad (2)$$

where μ_e and μ_g are the dipole moments in the excited and ground states, respectively, c is the velocity of light, h is the Plank's constant, and a_0 is the radius of the Onsager cavity around the fluorophore. Solvent dielectric constant (ε) and refraction index (n) are included in the term Δf, known as orientation polarizability. The Onsager radius was calculated from the optimized structure obtained by a semi-empirical calculation using PM3 method. The Onsager radius (3.61 Å) was taken as half of the average size of NI moiety. As shown in Fig. 4(B), the Stokes shift of a series of mixtures of 1,4-dioxane/CH_3CN changes linearly against the Δf, from which increases in the dipole moments ($\Delta\mu$) of 3.0–4.5 Debye for *p*-XYL:NI exciplexes were estimated (Table 1). Although the reason is presently not well understood, NI derivatives containing sulfur or oxygen show the large dipole-moment changes.

3.4. Time-resolved emission properties of exciplexes formed with p-XYL

Fig. 5 shows the time-resolved emission spectra of NI-C7 and NI-C8-PTZ in *p*-XYL/CH_3CN (v/v = 1:19), recorded in the region of 350–550 nm following the photoexcitation at 300 nm. In the early time range of 50 ps, the emission band around 380 nm which corresponds to the emission of $^1NI^*$ was observed together with the exciplex emission band around 450 nm. The decay of monomer $^1NI^*$ (τ_M; M denotes monomer compared with exciplex (E)) in *p*-XYL/CH_3CN was obviously very fast and almost within the present instrumental limit of ~50 ps. On the other hand, the τ_M in CH_3CN are 85–470 ps (Table 3) [4]. In *p*-XYL/CH_3CN, the shortening of τ_M implies the participa-

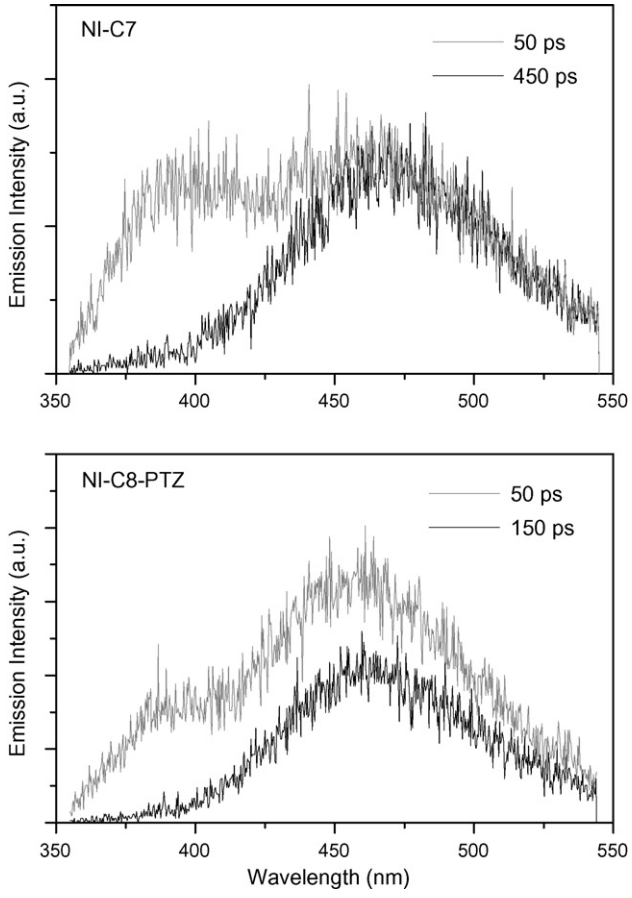

Fig. 5. Time-resolved emission spectra of NI-C7 (upper) and NI-C8-PTZ (bottom) observed at various times after a 100-fs 300-nm laser flash in *p*-XYL/CH_3CN (v/v = 1:19). Gray and black spectra are measured with delay time of 50 and 150 ps, respectively after the laser pulse excitation.

Table 3
Emission maxima (λ_{em} (nm)) and decay lifetimes of NI derivatives (τ_{em}) in CH_3CN and in *p*-XYL/CH_3CN

NI derivatives	CH_3CN		*p*-XYL/CH_3CN (v/v = 1:19)			
	λ_{em} (nm)	τ_M (ps)	λ_{em} (nm)	τ_M (ps)	τ_E (ns)	$\phi_{NI}/\phi_{NI\text{-}C}$
NI-C8-PTZ	378	85[a]	453	<50	0.38	0.22
NI-C11-PTZ	379	120[a]	454	<50	1.84	0.64
NI-O-PTZ	378	114[a]	457	<50	0.28	0.18
NI-C	378	195[a]	455	<50	3.32	1
NI-C7	379	138[a]	455	<50	3.02	0.68
NI-O	378	192[a]	458	<50	3.57	1.03
NI-O3	378	472	462	<50	3.22	0.77
NI-S	377	162	458	<50	1.66	0.31
NI-SOS	378	200	463	<50	2.17	0.75

τ_M and τ_E denote fluorescence lifetimes of monomeric NI derivatives and the exciplexes of NI derivatives and *p*-XYL.
[a] Data from ref. [4].

tion of fast deactivation process from $^1NI^*$. The reduced τ_M of $^1NI^*$ can be attributed to the formation of exciplex with *p*-XYL (*p*-XYL:NI)*. However, we could not resolve the formation time-constant of exciplex using both growth and decay temporal profiles for the exciplex and the monomer.

On the other hand, temporal emission profiles of exciplex were analyzed to fit exponential functions following a deconvolution procedure. The χ^2 values were within 1.1 for each system. The emission lifetimes of the exciplex (τ_E) were estimated to be 1.66–3.57 ns for reference NI-L derivatives. In cases of NI-C8-PTZ and NI-O-PTZ dyads, the τ_E were 0.38 and 0.28 ns, respectively. It is important to note that the exciplex emission band of NI-C8-PTZ was reduced quickly compared with that of NI-C7 as shown in Fig. 5. This strongly suggests that the exciplex emission is diminished by the quenching of PTZ. In contrast, we observed the τ_E values of 1.84 ns for NI-C11-PTZ dyad, which has a longer linker compared with NI-C8-PTZ or NI-O-PTZ. For the quenching process by PTZ, however, the PET via exciplex can be ruled out as discussed in the later section.

On the other hand, in pure *p*-XYL, the exciplex emission of NI derivatives at 450 nm was found to decay as a single exponential with a shorter lifetime compared with that in *p*-XYL/CH_3CN (Table 4). The solvent reorganization accompanying deactivation in both solvents may not be the same. Probably, the exciplex is probably more stable in polar solvent such as *p*-XYL/CH_3CN, because the exciplex has a charge transferred electronic character. Thus, the high emission quantum-yields for exciplex in *p*-XYL/CH_3CN can be anticipated compared with that in pure *p*-XYL as shown in Tables 3 and 4.

Table 4
Emission lifetimes (τ_{em}) and emission quantum yields (ϕ_{em}) of NI derivatives in *p*-XYL

NI derivatives	*p*-XYL	
	τ_{em} (ns)	ϕ_{em}
NI-C8-PTZ	0.31	0.005
NI-C11-PTZ	0.55	0.011
NI-O-PTZ	0.35	0.003
NI-C	0.70	0.021
NI-C7	0.53	0.016
NI-O	0.63	0.021
NI-O3	1.10	0.037
NI-S	0.56	0.009
NI-SOS	1.25	0.022

The relative ratios of the exciplex-emission quantum yield of NI derivatives against that of NI-C1 ($\phi_{NI}/\phi_{NI\text{-}C1}$) in *p*-XYL/$CH_3CN$ are listed in Table 3. The absolute exciplex-emission quantum yield ($\phi_{NI\text{-}C1}$) for NI-C1 was measured to be 0.034. The $\phi_{NI}/\phi_{NI\text{-}C1}$ values for NI-L-PTZ are smaller than those for reference NI derivatives (NI-L). This result is consistent with the change of emission lifetime for NI-L-PTZ. The

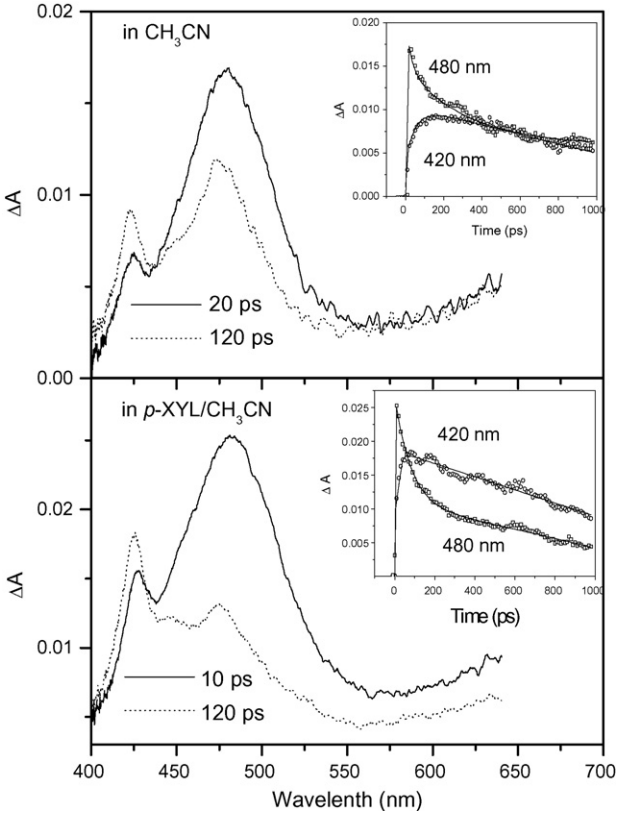

Fig. 6. Femtosecond time-resolved transient absorption of NI-C8-PTZ in CH_3CN (upper) and *p*-XYL/CH_3CN (v/v = 1:19) (bottom) after laser excitation (330 nm).

$\phi_{NI}/\phi_{NI\text{-}C1}$ for NI-C11-PTZ is larger than other dyads, implying that the exciplex efficiently formed rather than PET as well as other deactivation processes. Considering the linker effects, the relatively short linker length of NI-C8-PTZ and the electronic coupling through polyether linker of NI-O-PTZ can enhance the PET process compared with that of NI-C11-PTZ.

3.5. Transient absorption spectroscopic properties

Fig. 6 shows the transient absorption spectra of NI-C8-PTZ in *p*-XYL/CH_3CN and CH_3CN. At 10 ps after the excitation of NI-C8-PTZ with 130 fs duration pulse at 330 nm, two characteristic transient absorption bands were observed around 420 and 470 nm. These bands can be assigned to NI anion radical ($NI^{\bullet-}$) and S_1–S_n absorption band of NI [19]. In CH_3CN, the formation time constant of $NI^{\bullet-}$ for NI-C8-PTZ was ~78 ps. The formation time constants of $NI^{\bullet-}$ is similar to the fluorescence lifetimes of 85 ps for $^1NI^*$-C8-PTZ in CH_3CN (Table 2). It is noteworthy that the formation time constants of $NI^{\bullet-}$ correlate with the $^1NI^*$ lifetime. On the other hand, the formation time constant of $NI^{\bullet-}$ for NI-C8-PTZ in *p*-XYL/CH_3CN was quite short (~14 ps). Thus, it is concluded that the PET process occurred solely from $^1NI^*$, because the decay time constant (380 ps) of NI-C8-PTZ exciplex was much larger than the formation time constant of $NI^{\bullet-}$.

To examine the triplet excited state dynamics, we carried out nanosecond flash photolysis in *p*-XYL/CH_3CN under argon saturated condition (Fig. 7(A)). The absorption spectra for reference NI-C7 and NI-O3 recorded after photoexcitation at 355 nm are characterized by the T_1-T_n absorption around 470 nm (Fig. 7(A)). The triplet-state lifetimes of NI-C7 and NI-O3 were 2.94 μs for both at room temperature. The quantum yield of the triplet-state formation (ϕ_T) was estimated to be 0.88 and 0.79 for NI-C7 and NI-O3, respectively. In the case of NI-L-PTZ in *p*-XYL/CH_3CN, two characteristic transient absorption bands were observed around 420 and 520 nm as shown in Fig. 7(B). These bands can be assigned to $NI^{\bullet-}$ and $PTZ^{\bullet+}$, respectively, according to the previous reports [8,20,21].

Furthermore, the decay profiles of the $NI^{\bullet-}$ and $PTZ^{\bullet+}$ transient absorption of $NI^{\bullet-}$-L-$PTZ^{\bullet+}$ fitted using the bi-exponential components as shown in the insets of Fig. 7. From short-lived component of $NI^{\bullet-}$, the decay lifetimes of 107–830 ns and the rate constants (k_{CR}) of 1.2×10^7 to 9.3×10^6 s^{-1}, which are attributed to the intramolecular charge recombination (CR) process between $NI^{\bullet-}$ and $PTZ^{\bullet+}$ of $NI^{\bullet-}$-L-$PTZ^{\bullet+}$ were determined (Table 5). In addition, the long-lived

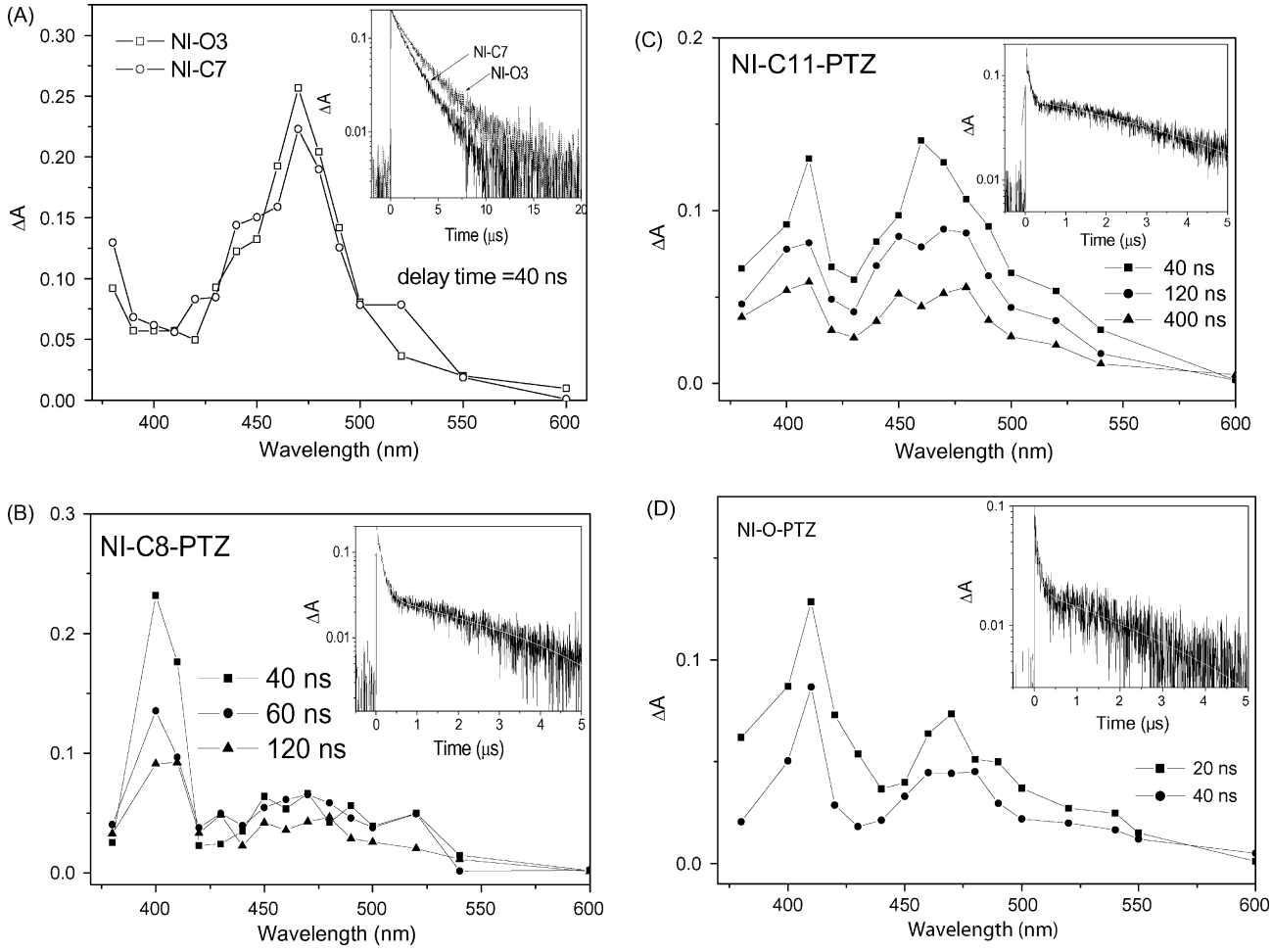

Fig. 7. Transient absorption spectra observed during the 355-nm ns-laser flash photolysis of reference compounds and dyads; (A) NI-C7 and NI-O3, (B) NI-C8-PTZ, (C) NI-C11-PTZ and (D) NI-O-PTZ in *p*-XYL/CH_3CN (v/v = 1:19). The inset shows kinetic traces of ΔA at 470 (A) and 420 nm (B–D).

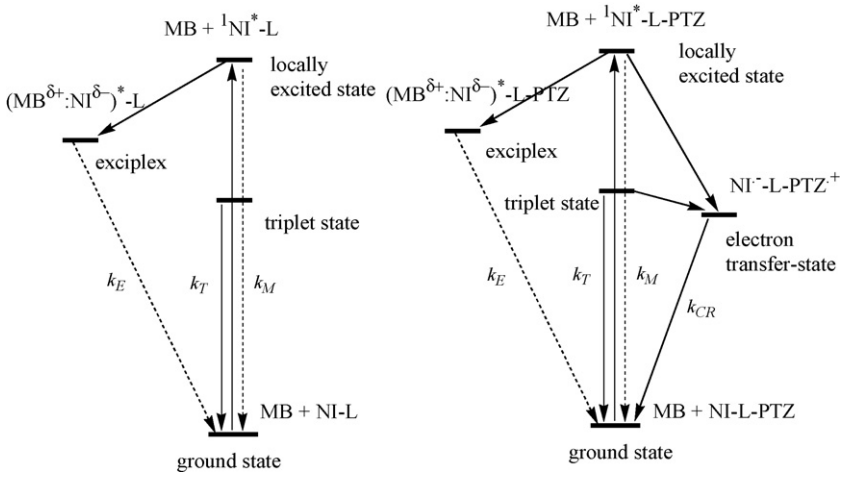

Scheme 2. Schematic representation of the photophysical process of NI-L-PTZ in MB.

components showed the decay lifetimes of 2.1–3.7 μs and the apparent rate constants of 2.7×10^5 to 4.7×10^5 s^{-1}. The trace long-lived components could be attributed to the intermolecular charge recombination process between radical ions $NI^{\bullet-}$-L-PTZ and NI-L-$PTZ^{\bullet+}$, generated from the bimolecular charge shift reaction between $NI^{\bullet-}$-L-$PTZ^{\bullet+}$ and NI-L-PTZ as reported in our previous work [4]. In *p*-XYL/CH_3CN, the CR rate constant depends on the concentration of NI-L-PTZ, because this may be the diffusion controlled process. On the other hand, the short-lived CR process in *p*-XYL/CH_3CN occurred quickly compared with those in CH_3CN. In our previous work, the CR rate increased with the decease in solvent polarity [4]. This indicates that the micro-environmental polarity around NI moiety in *p*-XYL/CH_3CN becomes less polar than in pure CH_3CN.

Based on the previous work [4], we suggest that the PET process of NI-C8-PTZ is efficient compared with that in NI-C11-PTZ because of a shorter linker. This suggestion is consistent with the fact that the triplet absorption at 470 nm in Fig. 7(B) is not evident than those in Fig. 7(C and D). Moreover, the efficient PET in NI-O-PTZ compared with that in NI-C11-PTZ reveals the strong electronic coupling through polyether linkers.

3.6. Mechanism

In MB, Scheme 2 depicted the deactivation mechanisms of NI-L-PTZ and reference NI in the excited states. From the steady-state emission spectra measured herein, we can propose that both reference NI and NI-L-PTZ derivatives formed the intermolecular exciplex with MB. The decay rate constants (k_M) of $^1NI^*$ in *p*-XYL/CH_3CN were larger than those in pure CH_3CN as shown in Table 3, because the exciplex formation serves as an important decay route in the deactivation process of $^1NI^*$. In 5% *p*-XYL/CH_3CN, the rate constant of exciplex formation could not be determined, because the excited NI is surrounded by a large number of *p*-XYL. In this case, the diffusion of NI within the lifetime of the excited state of NI (cf. Birks' scheme [22]) may be negligible. Therefore, the rising stage in the exciplex

Table 5
Rate constants of decay of NI^* (k_M, k_E and k_T, respectively), the charge recombination of $NI^{\bullet-}$-C-$PTZ^{\bullet+}$ and $NI^{\bullet-}$-O-$PTZ^{\bullet+}$ (k_{CR}) in *p*-XYL/CH_3CN

NI derivatives	Rate constants in *p*-XYL/CH_3CN (v/v = 1:19) (s^{-1})			
	k_M	k_E	k_T	k_{CR}[a]
NI-C8-PTZ	$>2 \times 10^{10}$	2.6×10^9	0	7.1×10^6 (3.6×10^6) 4.7×10^5 (2.6×10^5)
NI-C11-PTZ	$>2 \times 10^{10}$	5.4×10^8	0	9.3×10^6 (4.4×10^6) 3.7×10^5 (3.5×10^5)
NI-O-PTZ	$>2 \times 10^{10}$	3.6×10^9	0	1.2×10^6 (3.3×10^6) 2.7×10^5 (2.7×10^5)
NI-C	$>2 \times 10^{10}$	3.0×10^8	(2.6×10^5)	–
NI-C7	$>2 \times 10^{10}$	3.3×10^8	3.4×10^5 (3.7×10^5)	–
NI-O	$>2 \times 10^{10}$	2.8×10^8	(3.3×10^5)	–
NI-O3	$>2 \times 10^{10}$	3.1×10^8	3.4×10^5	–
NI-S	$>2 \times 10^{10}$	6.0×10^8	nd	
NI-SOS	$>2 \times 10^{10}$	4.6×10^8	nd	

[a] The charge recombination rates of $NI^{\bullet-}$ and $PTZ^{\bullet+}$ for $NI^{\bullet-}$-L-$PTZ^{\bullet+}$ were calculated from the decays of the transient absorption of $NI^{\bullet-}$ and $PTZ^{\bullet+}$. Parenthesis values in CH_3CN referred from ref [4].

decays may be absent, which should be originated from the diffusion. Moreover, the decay of $^1NI^*$-L-PTZ was faster than that of reference $^1NI^*$. NI-L-PTZ has been known to have the PET process as the deactivation of $^1NI^*$-L-PTZ which is one of competition progresses against the exciplex formation. While the PET process from the exciplex state is negligible, the formation rate constant of $NI^{\bullet-}$-L-$PTZ^{\bullet+}$ exhibits good correlation with the decay rate constant of $^1NI^*$-L-PTZ. Therefore, this implies that $NI^{\bullet-}$-L-$PTZ^{\bullet+}$ was directly generated from $^1NI^*$-L-PTZ. Thus, the PET process serves also as an important decay route in the deactivation processes of $^1NI^*$-L-PTZ dyads. Based on high emission quantum yield and the longer lifetime for exciplex, the PET process of NI-C11-PTZ is not an efficient process. This was explained by suggesting that the longer polymethylene linker of NI-C11-PTZ impedes the interaction between NI and PTZ moieties. As for the formation process of NI-L-PTZ exciplex, the deactivation process of NI-L-PTZ exciplex was also found to be linker dependent. Furthermore, NI-L-PTZ exciplex showed a quite fast decay compared with reference NI derivatives.

The decay rate constant (k_E) of $5.4 \times 10^8\ s^{-1}$ for NI-C11-PTZ exciplex is lower than other dyads ($2.6 \times 10^9\ s^{-1}$ in NI-C8-PTZ, and $3.6 \times 10^9\ s^{-1}$ in NI-O-PTZ). Based on femtosecond transient absorption studies, we already explained to the exclusion of the PET process as the quenching process of NI-L-PTZ exciplex. Although the reason for efficient quenching of NI-L-PTZ exciplex is not well understood, the quenching process of NI-L-PTZ exciplex could be affected by the presence of an appreciable interaction between NI and PTZ moieties. Considering the NI-L-PTZ structures connecting by flexible linkers, the strong static quenching of PTZ toward a NI moiety in the exciplex is expected to be somewhat relieved by the length and/or electronic character of linker.

4. Conclusions

The noticeable solvent effect for $^1NI^*$ is the formation of the exciplex with MB solvents. The intermolecular interaction between NI and MB allows charge transfer-type exciplex. The exciplex emission is affected by the solvent polarity, in accordance with the oxidation potential of MB. NI-L-PTZ dyads are linked by strong electron donor moiety (PTZ), so these dyads can attain to the PET in the excited state. The PET process in NI-L-PTZ serves as one of important decay route in the deactivation of $^1NI^*$. Extensive studies to reveal the PET of NI and related molecules in biosystem are in progress, because NI molecules have been applied to bio-systems as good electron acceptors.

Acknowledgements

This work has been partly supported by a Grant-in-Aid for Scientific Research (Project 17105005, Priority Area (417), 21st Century COE Research, and others) from the Ministry of Education, Culture, Sports, Science and Technology (MEXT) of Japanese Government. UCY acknowledges the Korea Ministry of Information and Communication (Center for Plastic Information System by ITRC program).

References

[1] I. Saito, M. Takayama, H. Sugiyama, K. Nakatani, A. Tsuchida, M. Yamamoto, J. Am. Chem. Soc. 117 (1995) 6406.
[2] K. Kawai, Y. Osakada, T. Takada, M. Fujitsuka, T. Majima, J. Am. Chem. Soc. 126 (2004) 12843.
[3] T. Takada, K. Kawai, S. Tojo, T. Majima, J. Phys. Chem. B 108 (2004) 761.
[4] D.W. Cho, M. Fujitsuka, A. Sugimoto, U.C. Yoon, P.S. Mariano, T. Majima, J. Phys. Chem. B 110 (2006) 11062.
[5] M.R. Wasielewski, Chem. Rev. 92 (1992) 435.
[6] D. Gust, T.A. Moore, A.L. Moore, Acc. Chem. Res. 26 (1993) 198.
[7] T.P. Le, J.E. Rogers, L.A. Kelly, J. Phys. Chem. A 104 (2000) 6778.
[8] G. Jones II, S. Kumar, J. Photochem. Photobiol. A: Chem. 160 (2003) 139.
[9] T.C. Barros, B. Filho, V.G. Toscano, M.J. Politi, J. Photochem. Photobiol. A: Chem. 89 (1995) 141.
[10] B. Abraham, L.A. Kelly, J. Phys. Chem. B 107 (2003) 12534.
[11] D.W. Cho, M. Fujitsuka, K.H. Choi, M.J. Park, U.C. Yoon, T. Majima, J. Phys. Chem. B 110 (2006) 4576.
[12] S.V. Rosokha, J.K. Kochi, J. Am. Chem. Soc. 123 (2001) 8985; S.M. Hubig, R. Rathore, J.K. Kochi, J. Am. Chem. Soc. 121 (1999) 617; S.M. Hubig, J.K. Kochi, J. Am. Chem. Soc. 121 (1999) 1688.
[13] S.L. Murov, I. Carmichael, G.L. Hug, Handbook of Photochemistry, second ed., Marcel Dekker, New York, 1993.
[14] M. Fujitsuka, A. Okada, S. Tojo, F. Takei, K. Onitsuka, S. Takahashi, T. Majima, J. Phys. Chem. B 108 (2004) 11935.
[15] I. Carmichael, G. Hug, J. Phys. Chem. Ref. Data 15 (1986) 54.
[16] K. Kawai, T. Takada, S. Tojo, T. Majima, Tetrahedron Lett. 43 (2002) 89.
[17] S.A. Alkaitis, G. Beck, M. Graetzel, J. Am. Chem. Soc. 97 (1975) 5723.
[18] V. Wintgens, P. Valet, J. Kossanyi, L. Biczok, A. Demeter, T. Berces, J. Chem. Soc., Faraday Trans. 90 (1994) 411.
[19] A. Smanta, G. Saroja, J. Photochem. Photobiol. A: Chem. 84 (1994) 19.
[20] J.E. Rogers, L.A. Kelly, J. Am. Chem. Soc. 121 (1999) 3854.
[21] T. Takada, K. Kawai, M. Fujitsuka, T. Majima, PNAS 101 (2004) 14002.
[22] J.B. Birks, Photophysics of Aromatic Moleculaes, Wiley, London, 1970.